ARCHIVES
of
FOUNDRY ENGINEERING

ISSN (2299-2944)
Volume 2025
Issue 3/2025

116 – 123

13/3

10.24425/afe.2025.155360

Published quarterly as the organ of the Foundry Commission of the Polish Academy of Sciences

Effect of Casting Parameters on the Structure and Properties of CuZn39Pb

M. Jabłoński
AGH University of Krakow, Poland
Corresponding author: E-mail address: jablonsk@agh.edu.pl

Received 21.10.2024; accepted in revised form 10.03.2025; available online 23.07.2025

Abstract

This paper reports the results of research on the effects of drawing speed on the structures and properties of leaded brass. The material used for the study was obtained via a laboratory horizontal continuous casting process. Horizontal continuous casting in a graphite mold represents a fast method for producing crystalline materials. In this process, molten metal crystallizes in a graphite mould on which a water-cooled copper jacket is applied. This step is often called primary cooling, as opposed to secondary cooling, which involves pouring water onto the surface of the rod using special nozzles. The crystallized rod is pulled out using a withdrawal unit (drawing speed). In brass, zinc causes the formation of alpha (α) and beta prim (β′) phases.
The effects of drawing speed on the structure and properties of brass rods obtained in the laboratory horizontal continuous casting process were analysed. The chemical composition, macrostructure, microstructure, mechanical properties, surface roughness and conductivity properties were investigated. An increase in the drawing speed in the analysed range causes a refinement of the microstructure and growth of the grain boundaries. As the grain size decreases, the Vickers hardness and proof stress ($R_{p0.2}$) of the cast brass increase, the total extension at fracture (A_t), and the surface quality decrease.

Keywords: Horizontal continuous casting process, CuZn39Pb3 alloy, Mechanical properties, Microstructure of brass

1. Introduction

Pure copper has good electrical and thermal properties and is thus used as a conductor [1-3]; however, unfortunately, it is expensive and soft and has good ductility. However, the mechanical properties and corrosion resistance of pure copper can be improved by alloying with elements such as Zn, Sn, Ni, Si, Fe, and Mn [4-7]. Copper and copper alloys are commonly used in architecture, automotive, electrical, industrial, marine, etc. The most common copper alloys are brasses, for which zinc is the predominant alloying element. Cu-Zn alloys have good mechanical properties, high corrosion resistance and good machinability. The brass can be divided into mono-phases and poly-phases. The alpha (α) phase of brass is stable at concentrations up to approximately 35% by weight of Zn. This phase has a fcc crystal structure and is relatively soft, ductile and easily cold worked. The strength and ductility of these alloys increase with increasing zinc content. The alpha alloys can be differentiated by a gradual change in colour, from golden yellow to red, as the zinc content increases up to 35% by weight. Brass alloys with a higher Zn content resemble both the alpha and beta prim (β′) phases at room temperature. The β′ phase has an ordered bcc crystal structure and is harder and stronger than the α phase. The ratio of the alpha to beta prim phase depends principally upon the zinc content. The presence of the beta prim phase in the α + β′ brass gives rise to reduce cold ductility but

greatly increases the ability to hot work by extrusion, stamping or die casting without hot cracking. Brasses have excellent castability and a good combination of strength and corrosion resistance [8].

In this research, brass, which had 58.52 - 58.98% by weight of Cu, 2.742 - 2,756% by weight of Pb, Sn less than 0.15% by weight, and Fe less than 0.17% by weight, was used, and the remaining elements, such as Ag, Al, As, Bi, Cd, Co, Cr, Mg, Mn, Ni, P, S, Sb, Si, and Zr, were less than 0.1% by weight. Hence, this alloy was classified as CuZn39Pb3 (CW614N) according to the established standard PN-EN 12164. This alloy is often referred to as C38500 (USA) or MO58A (PN) depending on the standards. The addition of lead to these alloys is to improve machinability and aids chip breakage during machining, producing short broken chips that are easily cleared from the cutting area. Moreover, the addition of Pb increases productivity, lowers cutting forces and extends tool life. Lead does not form a solid solution with copper or zinc but is present as a dispersed discontinuous phase distributed at grain boundaries [9-11]. Many studies have been conducted on the effects of cooling rate, solidification, and drawing speed on the microstructures and properties of brass [12-16]. Depending on the casting conditions, chemical composition, modifiers and presence of trace elements, materials with different structures and properties can be obtained [17-20]. The solid solubility of Zn in the Cu matrix is very high, resulting in α and β′ -phases. In addition, the presence of other trace elements can also influence the phase evolution significantly.

In this study, the author tried to examine the effect of drawing speed on the properties and structure leaded brass. The chemical composition, macrostructure, microstructure, mechanical properties, electrical properties and quality of the surface cast rods were studied.

2. Methods

The material used for testing was obtained via a laboratory horizontal continuous casting process using a graphite crystallizer (Fig. 1) [21]. The input to the process of laboratory casting was brass scraps with known chemical compositions. Approximately 30 kg of brass scrap was melted in 30 minutes in an induction furnace without a protective atmosphere. The furnace was equipped with a 20 kW power generator, which ensured the continuity of the casting process using the horizontal crystallization system of primary and secondary cooling. After the melting process, a continuous casting process was carried out with different drawing speed (Table 1). As a result, four ingots with a diameter of 10 mm were obtained. Figure 2 shows the surface of the cast ingots.

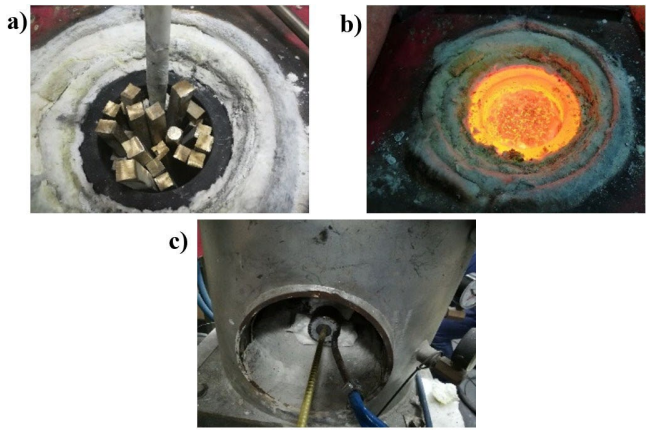

Fig. 1. View of scrap metal placed in a graphite crucible (a), view of molten metal in crucible (b) and view from the crystallizer side (c)

Table 1.
Parameters of the horizontal continuous casting process

Number of ingot	I	II	III	IV
Drawing speed [mm/s]	1	10	15	20
Stoppage [s]	1	5	5	5
Temperature of liquid metal [°C]	1020	1020	1030	1040
Temperature of primary cooling metal [°C]	165	170	205	220
Temperature of secondary cooling metal [°C]	32	32	34	36
Temperature of primary cooling water [°C]	10	10	11	12
Temperature of secondary cooling water [°C]	8	8	9	10
Velocity of primary cooling water [l/min]	1.5			
Velocity of secondary cooling water [l/min]	0.5			

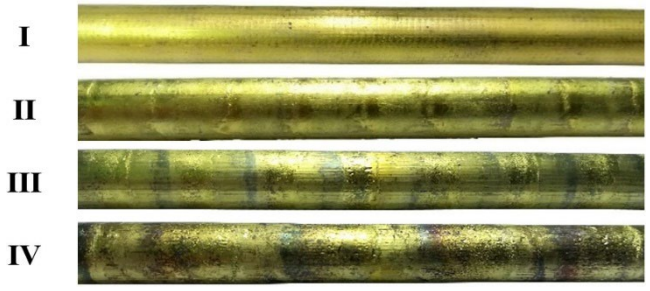

Fig. 2. The surface of the cast ingots

The next step of the research was to measure the composition of the ingots, which were obtained via optical mass spectrometry. At least five spark analyses were performed for each sample, and the average value was taken as the chemical composition of the ingot. The standard deviation did not exceed 1 % of the average value for each chemical element. The actual compositions of the alloys are shown in Table 2. The tested material was consistent with

the requirements of the PN-EN 12164:2016 standard and was designated CW614N (CuZn39Pb3).

Table 2.
Chemical composition of ingots casted with different parameters (wt.%)

Number of ingot	Cu	Zn	Pb	Sn	Fe	Other*
I	58.52	38.32	2.754	0.145	0.165	0.096
II	58.74	38.11	2.747	0.139	0.165	0.099
III	58.79	38.06	2.756	0.137	0.163	0.094
IV	58.98	37.89	2.742	0.138	0.161	0.089

*Ag, Al, As, Bi, Cd, Co, Cr, Mg, Mn, Ni, P, S, Sb, Si, Zr

The next step was to observe the microstructure of the cast rods at various magnifications using stereo (ZEISS Stemi 508) and light microscopy (ZEISS AxioVert.A1). A detailed analysis of the microstructural features of the selected ingots was performed by scanning electron microscopy (SEM) instrument equipped with an energy dispersive X-ray spectroscopy (EDS) detector. The metallographic samples were prepared by catting, mounting in acrylic resin and grinding with silicon carbide grit papers of 300, 600, 1000, 2000 and 4000, in the presence of water and then polished with diamond paste on disk polishing machine. These samples were etched before inspection under optical microscope by immersing into etching solution with consist of 10 g of $FeCl_3$, 10 ml of HCL and 90 ml of H_2O.

The tensile tests were conducted following the ISO 6892-1:2019 standard using a Zwick Z020 testing machine equipped with testXpert Testing Software and a 20 kN load cell. All the tests were performed at room temperature (~20°C). The gauge length of the extensometer was 50 mm, and the ramp rate for extension was 50 mm/min. The tensile strength (R_m), proof stress or proof strength ($R_{p0.2}$) and percentage total extension at fracture (A_t) were determined from these measurements. R_m is the stress corresponding to the maximum force, $R_{p0.2}$ is the stress at which the plastic extension is equal to 0.2% of the extensometer gauge length, and A_t is the elastic extension plus plastic extension at the moment of fracture, expressed as a percentage of the extensometer gauge length. Five measurements for each ingot were performed, after which the arithmetic mean and standard deviation were calculated.

The Vickers hardness test was conducted following the ISO 6507-1:2023 standard using a Tukon 2500 testing machine equipped with a Minuteman hardness test program and a 5 kgf load cell. All the tests were performed at ambient temperature (~20°C). Five hardness measurements were performed, after which the arithmetic mean was calculated. Moreover, the estimated standard deviation was also calculated.

The electrical conductivity of the ingots was determined using a RESISTOMAT® model 2304 (Burster Company). These testing instruments use the 4-wire measurement method designed by Kelvin to cancel any resistance errors. The resistance of the sample was measured based on Ohm's law. By knowing the measurement length and diameter, the resistivity was determined. The inverse of the resistivity is the electrical conductivity. The tests were performed at room temperature, and the measurement error was less than 0.01%. Five measurements were performed, after which the arithmetic mean and standard deviation were calculated.

The quality of the surface of the cast rods was determined using a Hommel-Etamic T1000 testing machine following the ISO 21920-1:2021. This mobile device was equipped with a skid probe (T1E) for determining the roughness, waviness and profile parameters. The measurement range was 80 µm, the length of measurement was 4.8 mm, and the cut-off value was 0.25 mm. Five roughness measurements were made on each sample along the axis of symmetry of the rod, after which the arithmetic mean was calculated. The average roughness (R_a) and ten-point height of irregularities (R_z) were selected to evaluate the surface roughness. R_a is the arithmetic average of the absolute values of the profile heights over the evaluation length, and R_z is the average value of the absolute values of the heights of the five highest-profile peaks and the depths of the five deepest alleys within the evaluation length.

3. Results and Discussion

By selecting appropriate casting speed, it was possible to maintain the continuity of the cast rods and good surface quality. Figure 2 shows the surface quality of the cast ingots. Sample no. 1 had the best surface quality obtained for ingot I. In each case, transverse lines could be observed on the surface of the cast rods, which indicate the material joining zone. Increasing the drawing speed from 1 to 20 mm/s and stopping during casting from 1 to 5 seconds did not seem to reduce the surface quality. Additionally, good surface quality was obtained for ingot no. IV even though it was heavily oxidized during crystallization. The alloy obtained during the horizontal continuous casting process without a protective atmosphere met the chemical composition requirements and was classified as CuZn39Pb3 (CW614N). During the casting process, the temperature of the liquid metal increased, which resulted in an increase in the temperature of the primary cooling metal (Table 1). Controlling the temperature of the liquid metal is extremely important for preventing overheating of the molten metal and excessive zinc evaporation. A slight decrease in the zinc content in the alloy was observed during the casting process from 38.32 to 37.89 wt.% as a result of the burning off of zinc. Moreover, attention was given to the low amount of impurities (see Table 2). The next step was to study the macrostructure of these ingots. Figure 3 shows the cross-section and longitudinal section of the macrostructure of CuZn39Pb3. The largest a refinement of the macrostructure (fine-grained structure) was noted for ingot no. IV, while the coarse structure was noted for ingot no. I (comparing the longitudinal section). The casting speed and stoppage were correctly selected, which confirmed that the crystallization of the core in the middle of the ingots was especially noticeable for ingot no. 3. In turn, for ingot no. 2, we observed a herringbone structure.

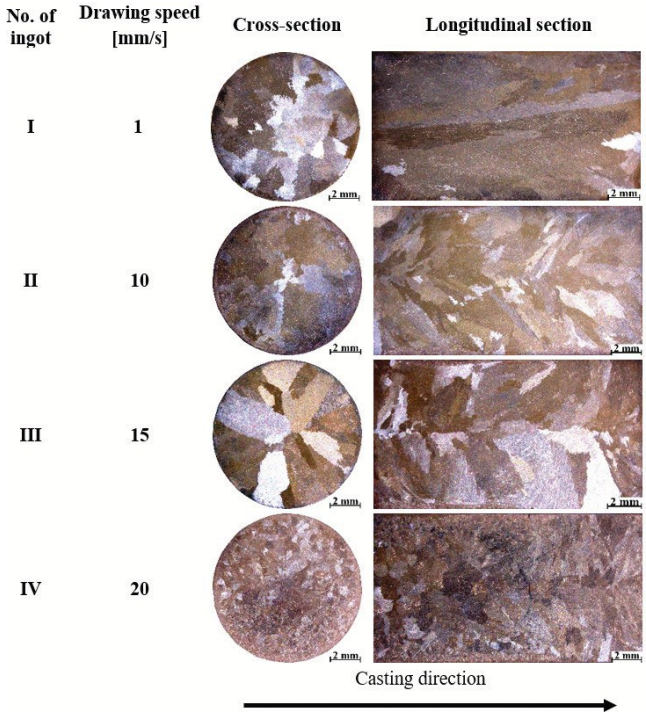

Fig. 3. The macrostructure of ingots. Cross-section on the left side and longitudinal section on the right side with the casting direction marked

Figure 4 shows the typical foundry microstructure of CuZn39Pb3 at 50x magnification under brightfield (BF) and polarized light (PL) conditions. We observed dendritic microstructures for all ingots. These photos reveal the occurrence of two-phase solid solution Zn in Cu (the α direction is bright) and solid solution Cu in Zn (the β′ direction is dark). In the images taken under polarized light, we observe dendrites oriented in the same crystallographic direction.

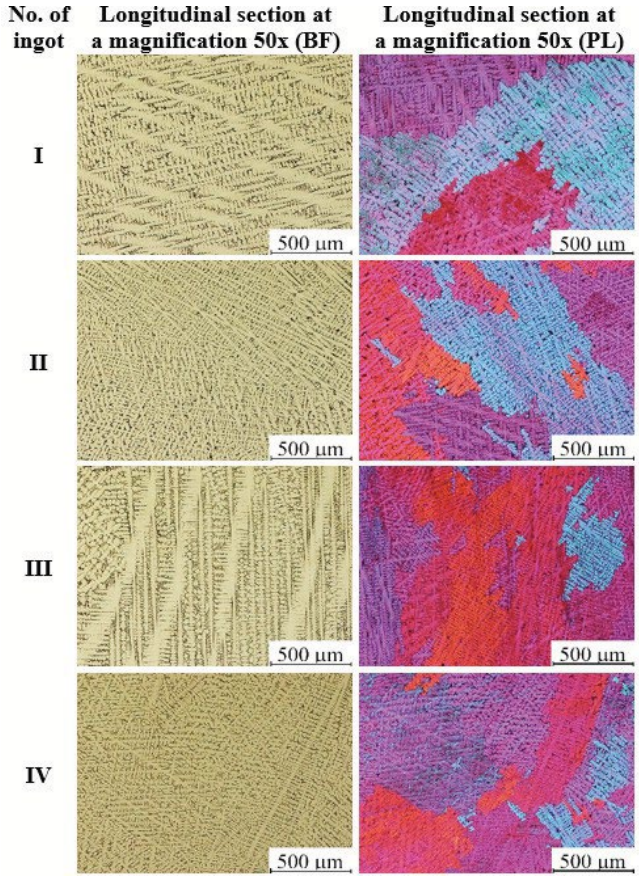

Fig. 4 Optical microscope images of the longitudinal section microstructure of ingots at a magnification of 50x. Bright field (BF) on the left side and polarized light (PL) on the right side

In turn, Figure 5 shows the microstructure of the cast brass magnifications of 200x and 500x. The longitudinal surface of the bars between the center and the edge of the sample was observed. Attention was given to the strongly heterogeneous microstructure with different amounts of α and β′ phases. The visible black points at 500x magnification are located at the phase boundaries where the dispersive precipitates are lead, which is insoluble in zinc and copper. The presence of the α and β′ phases as well as Pb was confirmed by scanning electron microscope (SEM). Figure 6 shows the microstructure of cast ingot no. I, which was observed using SEM in backscattered electron (BSE) mode. A similar microstructure was observed for the remaining ingots, so it was decided not to publish these photos. These observations confirmed the existence of two phases, α and β′. Moreover, the occurrence of Pb precipitates was observed (bright points in BSE mode). Chemical characterization via energy-dispersive spectroscopy (EDS) confirmed the presence of the α phase with a zinc concentration up to ~34 % by weight, and β′ phase ~43% by weight of Zn and particles of Pb (see Figure 7 Table 3 and Figure 8 Table 4). Lead occurs on the grain border and between dendrites. A homogeneous distribution of Pb helps to fragment the microstructure.

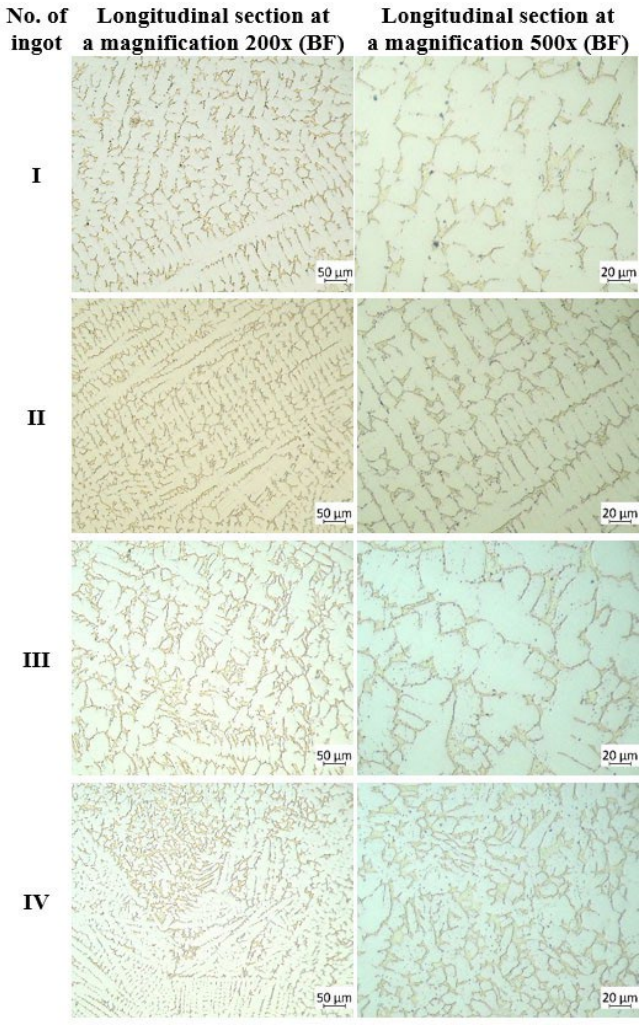

Fig. 5. Optical microscope images of longitudinal section microstructures of ingots at magnifications of 200x on the left side and 500x on the right side

Table 3.
Chemical composition of ingot no. I in in the central part of the sample (wt.%)

Point	Cu	Zn	Pb
1	56.58	43.42	-
2	65.83	34.17	-
3	26.41	13.77	59.82

Table 4.
Chemical composition of ingot no. I at the edge of the sample (wt.%)

Point	Cu	Zn	Pb
1	14.19	8.16	77.65
2	57.83	42.17	-
3	64.91	35.09	-

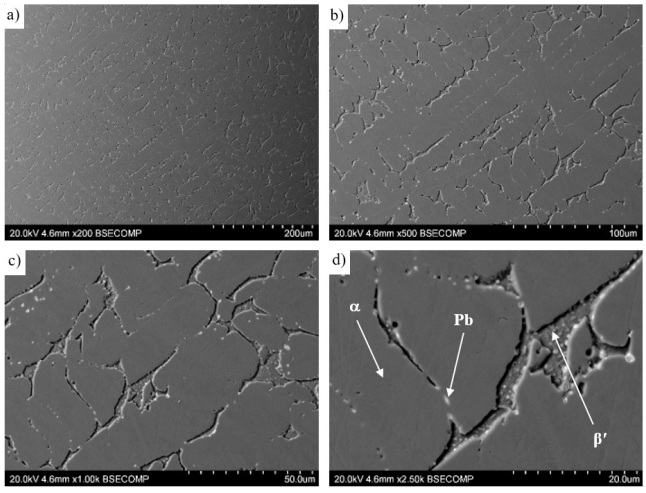

Fig. 6. SEM images of ingot no. I obtained using BSE mode at magnifications of 200x (a), 500x (b), 1000x (c) and 2500x (d)

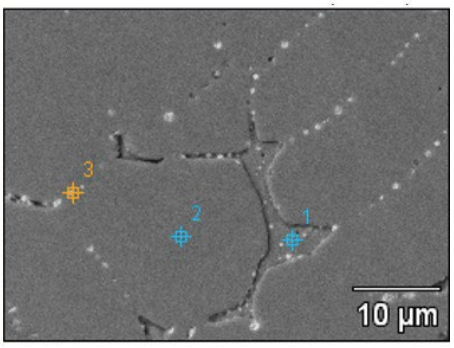

Fig. 7. SEM image and points of chemical composition of ingot no. I in the central part of the sample

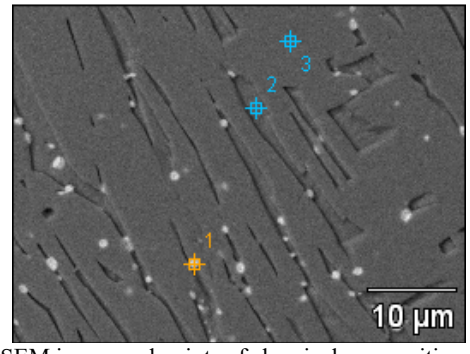

Fig. 8. SEM image and points of chemical composition of ingot no. I at the edge of the sample

The engineering stress as a function of engineering strain curves of the cast ingots is shown in Figure 9. No characteristic portevin-Le Chatelier (PLC) effect was observed for this material. The PLC effect describes a serrated stress-strain curve that some materials exhibit as they undergo plastic deformation (discontinuous plastic flow) [22]. Selected mechanical properties are shown in Figure 10. For drawing speed from 1 to 20 mm/s we observe a decrease in R_m of 1.03 and At of 1.38 and an increase in

$R_{p0.2}$ of 1.08. Changes in the properties were the result of differences in the microstructure and surface quality due to differences in the crystallization conditions (Table 1). In general, an increase in the drawing speed in a given range results in an increase in the mechanical properties ($R_{p0.2}$) and a decrease in the plastic properties (A_t) due to refinement of the microstructure. The observed decrease in tensile strength (R_m) from ingot 2 to 4 may be due to the decrease in surface quality. A shorter residence time of the metal in the primary cooling zone causes defects in the form of short run casting (structure discontinuities), which may constitute stress concentrators in a tensile test, consequently leading to faster cracking of the ingot. Moreover, an increase in the temperature of primary cooling metal was notice due to the fact that the metal remains in the primary cooling zone for a shorter time and thus there is less heat absorption by water. The standard deviation did not exceed 2 % of the average value.

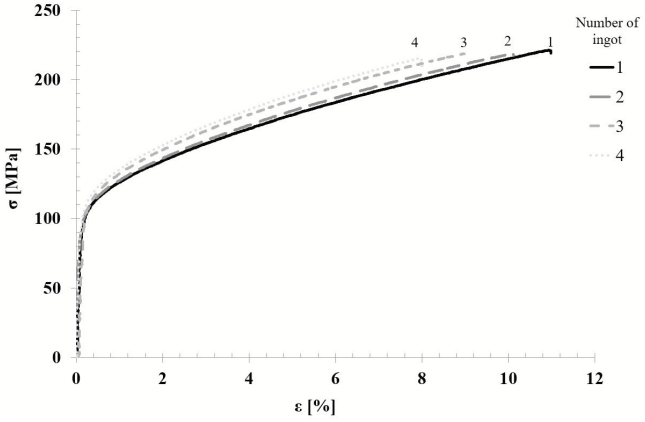

Fig. 9. Stress-strain curves of the cast ingots

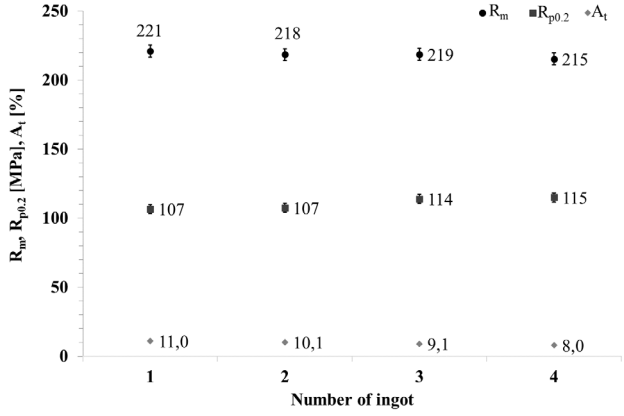

Fig. 10. Mechanical properties of the cast ingots

Figure 11 shows the Vickers hardness for ingot castings with different parameters. An increase in the drawing speed causes an increase in the hardness above 1.18 as a result of refinement of the structure (see Figure 3). The standard deviation did not exceed 4 % of the average value. The wide dispersion of the values from the average value may be caused by differences in crystallization conditions, which directly resulted in the differentiation of the structure between the center and the edge of the ingot.

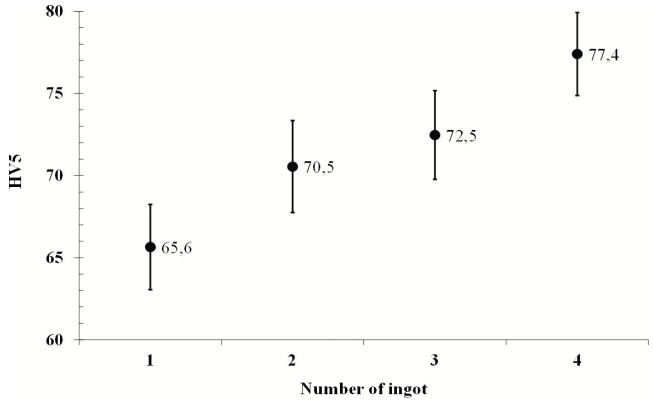

Fig. 11. The Vickers hardness (HV5) of the cast ingots

An increase in a refinement of the microstructure and hardness due to an increase in drawing speed will likely translate into a decrease in the electrical conductivity of the cast ingots. A slight increase in conductivity of 1.02 was observed (Fig. 12), which may indicate a smaller share of the β′ phase in the alloy, which is more rich in zinc than the α phase. The lower content of zinc in the tested alloy results from its evaporation during casting, i.e., the alloy contains more copper. In conclusion, we observe a synergistic effect of several factors (structure discontinuities, fine-grained structure, impurities), of which the evaporation during casting is the most important and determines the increase in electrical conductivity. The standard deviation did not exceed 0.02 % of the average value.

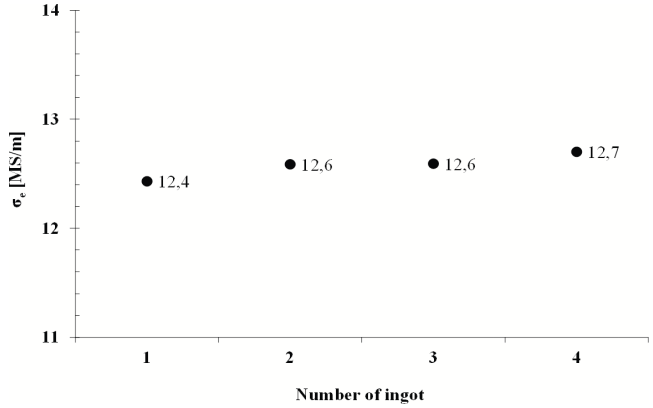

Fig. 12. The electrical conductivity (σ_e) of the cast ingots

At the end of the research, it was decided to examine the influence of drawing speed on the surface quality of the ingots, and it was found that with the increasing drawing speed, the surface roughness increased, i.e., its quality deteriorated, which was confirmed by Figure 2. For both R_z and R_a, the standard deviation did not exceed 10 % of the average value (Figure 13).

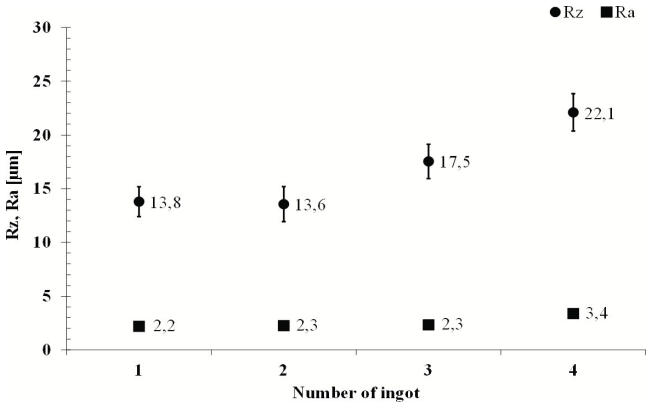

Fig. 13. The surface roughness (Rz , Ra) of the cast ingots

4. Conclusions

The aim of this work was to examine the effect of drawing speed from 1 to 20 mm/s on the macrostructure, microstructure, mechanical properties, electrical properties and surface quality of a CuZn39Pb3 alloy obtained via a laboratory horizontal continuous casting process. The selection of casting conditions is extremely important in the context of the efficiency of the process, material properties and surface quality of the cast rods. During the casting process, the mass of the molted metal decreases, which affects the reduction of the hydrostatic pressure in the crucible, and thus changes the condition of the flow of the liquid metal to the crystallization zone. Another aspect is the increase in the liquid metal, which directly affects the growth of the temperature in the crystallizer. High temperature translates into burning off of zinc, whose melting point is much lower than copper.

This special brass is susceptible to hot forging and machining, but cold forming is difficult. Lead, which is practically insoluble in brass, is released in the form of inclusions mainly at grain boundaries. Moreover, it lowers the melting point and increases the castability of brass. In turn, the addition of iron to the tested alloy inhibited hot cracking. On the basis of the conducted research, the following conclusions can be drawn:

- Changing the drawing speed from 1 to 20 mm/s resulted in an increase in a refinement of the microstructure, Vickers hardness, and proof stress ($R_{p0.2}$) and a decrease in total extension at fracture (A_t), surface quality (Rz, Ra),
- Increasing the casting speed from 1 to 20 mm/s causes a decrease in tensile strength most likely as a result of structure discontinuities which may constitute stress concentrators in a tensile test leading to faster cracking of the ingot,
- It was possible to cast an alloy under laboratory conditions with a chemical composition that meets the requirements of the standard, appropriate properties and satisfactory surface quality,
- The ingots are characterized by a typical foundry structure (dendric structure) with α+β′ phase and dispersive Pb precipitation occurring at the phase boundary,
- The slight increase in the electrical conductivity of the ingots during casting could be explained by zinc evaporation and thus the increase in the presence of copper, but impurities are also a possible contributor.

Further tests for deformability in the laboratory hot forging process of components for the electrical industry are planned.

References

[1] Lu, L., Shen, Y., Chen, X., Qian, L. & Lu, K. (2004). Ultrahigh strength and high electrical conductivity in copper. *Science.* 304(5669), 422-426. DOI: 10.1126/science.1092905.

[2] Han, D., Kim, G.-H., Kim, J. & Ahn, B. (2020). Effect of Al/Cu weight fraction on the mechanical and electrical properties of Al-Cu conductors for overhead transmission lines. *Archives of Metallurgy and Materials.* 65(3), 1019-1022. DOI: 10.24425/amm.2020.133210.

[3] Hu, H., Yan, J., Sævik, S., Ye, N., Lu, Q. & Bu, Y. (2022). Nonlinear bending behavior of a multilayer copper conductor in a dynamic power cable. *Ocean Engineering.* 250, 110831, 1-11. DOI: 10.1016/j.oceaneng.2022.110831.

[4] Piekoś, M., Garbacz-Klempka, A., Kozana, J. & Żak, P.L. (2020). Impact of Ti and Fe on the microstructure and properties of copper and copper alloys. *Archives of Foundry Engineering*. 20(4), 83-90. DOI: 10.24425/afe.2020.133352.

[5] Rzadkosz, S., Garbacz-Klempka, A., Kozana, J., Piekoś, M. & Kranc, M. (2014). Structure and properties research of casts made with copper alloys matrix. *Archives of Metallurgy and Materials.* 59(2), 775-778. DOI: 10.2478/amm-2014-0131.

[6] Kranc, M., Sikora, G., Górny, M. & Garbacz-Klempka, A. (2017). The influence of Mg additive on the structure and electrical conductivity of pure copper castings. *Archives of Foundry Engineering*. 17(4), 85-90. DOI: 10.1515/afe-2017-0135.

[7] Krupińska, B., Chulist, R., Kondracki, M. & Labisz, K. (2023). Thermoplastic hardened Cu-Ni-Si-Ag alloy. *Bulletin of the Polish Academy of Sciences. Technical Sciences.* 71(2), 85-90. DOI: 10.24425/bpasts.2023.145683.

[8] Stavroulakis, P., Toulfatzis, A.I., Pantazopoulos, G.A. & Paipetis, A.S. (2022). Machinable leaded and eco-friendly brass alloys for high performance manufacturing processes: A critical review. *Metals*. 12(2), 246, 1-31. DOI: 10.3390/met12020246.

[9] Hsieh, C., Wang, J., Wu, P.T. & Wu, W. (2013). Microstructural development of brass alloys with various Bi and Pb additions. *Metals and Materials International*. 19, 1173-1179. DOI: 10.1007/s12540-013-6002-2.

[10] Pantazopoulos, G. (2002). Leaded brass rods C38500 for automating machining operations: A technical report. *Journal of Materials Engineering and Performance.* 11(4), 402-407. DOI: 10.1361/105994902770343926.

[11] Atsumi, H., Imai, H., Li, S., Kondoh, K., Kousaka, Y. & Kojima, A. (2012). Fabrication and properties of high-strength extruded brass using elemental mixture of Cu-40% Zn alloy powder and Mg particle. *Materials Chemistry and Physics*. 135(2-3), 554-562. DOI: 10.1016/j.matchemphys.2012.05.025.

[12] Biernat, S. & Bydałek, A.W. (2014). Optimization of the brass melting. *Archives of Foundry Engineering.* 14(3), 5-10. DOI: 10.2478/afe-2014-0051.

[13] Kwapisiński, P., Lipnicki, Z., Ivanova, A.A. & Wolczyński, W. (2017). Role of the structural and thermal peclet numbers in the brass continuous casting. *Archives of Foundry Engineering.* 17(2), 49-54. DOI: 10.1515/afe-2017-0050.

[14] Wolczyński, W., Lipnicki, Z., Bydałek, A.W. & Ivanova, A.A. (2016). Structural zones in large static ingot. Forecasts for continuously cast brass ingot. *Archives of Foundry Engineering*. 16(3), 141-146. DOI: 10.1515/afe-2016-0067.

[15] Anakhov, S. & Fominykh, S. (1997). Effect of the cooling rate after remelting on the structure of antifriction brass. *Metal Science and Heat Treatment*. 39(6), 240-243. DOI: 10.1007/bf02467227.

[16] Kwaśniewski, P., Najman, K., Wolczyński, W., Bydałek, A.W. & Schlafka, P. (2018). Determination of the technological parameters process for continuously cast brass ingot. *Archives of Foundry Engineering*. 18(10), 9-14. DOI: 10.24425/118803.

[17] Chen, W., Jia, Y., Jiang, Y., Wang, M., Derby, B. & Lei, Q. (2017). Effect of addition of Ni and Si on the microstructure and mechanical properties of Cu–Zn alloys. *Journal of Materials Research*. 32(16), 3137-3145. DOI: 10.1557/jmr.2017.145.

[18] Greß, T., Nardi, V.G., Mittler, T., Schmid, S., Buchberger, P., Tonn, B. & Volk, W. (2019). Interface formation and characterization of brass/aluminum compounds fabricated through die casting and semi-continuous casting. *International Journal of Metalcasting*. 14(2), 564-579. DOI: 10.1007/s40962-019-00387-0.

[19] Wolczyński, W. (2018). Nature of segregation in the steel static and brass continuously cast ingots. *Archives of Metallurgy and Materials*. 63(4), 1915-1922. DOI: 10.24425/amm.2018.125124.

[20] Bydałek, A.W., Kula, A., Błaż, L. & Najman, K. (2019). Analysis of the impact of modifiers on the formation of non-metallic inclusions during continuous casting of CuZn39Pb2 brass. *Archives of Foundry Engineering.* 19(3), 21-26. DOI: 10.24425/afe.2019.127132.

[21] Jabłoński, M., Knych, T., Mamala, A. & Palczewski, M. (2015). Influence of casting velocity on structure and properties of AlFe0,5 alloy. *Key Engineering Materials*. 641, 56-62. DOI: 10.4028/www.scientific.net/kem.641.56.

[22] Cottrell, A. (1953). LXXXVI. a note on the portevin-le chatelier effect. *The London, Edinburgh, and Dublin Philosophical Magazine and Journal of Science*. 44(355), 829-832. DOI: 10.1080/14786440808520347.